A lognormal distribution of the lengths of terminal twigs on self-similar branches of elm trees

Kohei Koyama[1], Ken Yamamoto[2,3] and Masayuki Ushio[4,5,6,7]

[1]Department of Life Science and Agriculture, Obihiro University of Agriculture and Veterinary Medicine, Inada-cho, Obihiro 080-8555, Japan.

[2]Department of Physics, Faculty of Science and Engineering, Chuo University, Bunkyo, Tokyo 112-8551, Japan.

[3]The present address: Department of Physics, Faculty of Science, University of the Ryukyus, Senbaru, Nishihara, Okinawa 901-0213, Japan.

[4]Department of Environmental Solution Technology, Faculty of Science and Technology, Ryukoku University, 1-5 Yokotani, Seta Oe-cho, Otsu 520-2194, Japan.

[5]Joint Research Center for Science and Technology, Ryukoku University, 1-5 Yokotani, Seta Oe-cho, Otsu 520-2194, Japan

[6]The present address-1: Center for Ecological Research, Kyoto University, 2-509-3 Hirano, Otsu, Shiga 520-2113, Japan.

[7]The present address-2: PRESTO, Japan Science and Technology Agency, 4-1-8 Honcho, Kawaguchi, Saitama 332-0012, Japan.

Author for correspondence:

Kohei Koyama

e-mail:koyama@obihiro.ac.jp

Abstract

Lognormal distributions and self-similarity are characteristics associated with a wide range of biological systems. The sequential breakage model has established a link between lognormal distributions and self-similarity and has been used to explain species abundance distributions. To date, however, there has been no similar evidence in studies of multicellular organismal forms. We tested the hypotheses that the distribution of the lengths of terminal stems of Japanese elm trees (*Ulmus davidiana*), the end products of a self-similar branching process, approaches a lognormal distribution. We measured the length of the stem segments of three elm branches and obtained the following results: (1) each occurrence of branching caused variations or errors in the lengths of the child stems relative to their parent stems; (2) the branches showed statistical self-similarity; the observed error distributions were similar at all scales within each branch; and (3) the multiplicative effect of these errors generated variations of the lengths of terminal twigs that were well approximated by a lognormal distribution, although some statistically significant deviations from strict lognormality were observed for one branch. Our results provide the first empirical evidence that statistical self-similarity of an organismal form generates a lognormal distribution of organ sizes.

Keywords: allometry, fractal, phenotypic plasticity, shoot size, stochastic process, WBE theory

1. Introduction

Modelling individual and ecosystem metabolism is one of the central goals of ecophysiology [1-7]. There have been two distinct approaches to modelling the metabolism (respiration or photosynthesis) of individual plants. One approach is to use biological scaling theories, which focus on allometric (i.e., power-law) relationships between organismal size and metabolism [8-15]. Among biological scaling theories, metabolic scaling theories [8-11], which are based on the self-similarity of plant vascular networks, are one of the most successful approaches, because they enable modelling of metabolism from individuals to ecosystems [10, 16, 17]. The other approach is to use canopy optimization models [18-20], which consider whole plants or stands of plants as a heterogeneous set of terminal organs (e.g., leaves). The optimization models are based on theoretical arguments [18-21] and observations [18, 22, 23] that terminal organs show plasticity in terms of size, function, and direction (e.g., leaf angle), and that this plasticity increases whole-plant photosynthetic rates. The use of optimization models has also been a standard approach for modelling ecosystem carbon gain [19, 20].

These two approaches have been equally successful, but to date the synergism of the two approaches has not been achieved. Previous biological scaling theories, such as metabolic scaling theories, ignore the phenotypic plasticity of terminal organs and instead make the simplifying assumption that the size and function of terminal organs (such as twigs or leaves) are invariant within individual organisms [e.g., 1, 3, 4, 8, 9, 13, 14, 16, 17, 24, 25]. In contrast, optimization models [19, 20] consider each set of terminal organs within a given space as a canopy and ignore the fact that those terminal organs are connected to a self-similar resource transportation network and that they are part of an individual plant that obeys allometric relationships. Hence, there has been a discrepancy

between metabolic scaling theories and canopy optimization models. Enquist and Bentley [10] have suggested that taking account of the variability of the size of terminal organs will improve present metabolic scaling theories. Smith et al. [26], as well as Hunt and Savage [27], have analysed how plasticity of branching morphology affects individual metabolism. However, to date current biological scaling theories have not successfully modelled plasticity of terminal organs.

The distributions of size in biology have often been approximated by lognormal distribution functions [28-34]. The use of lognormal distributions can be rationalized in part by a mathematical model called the sequential breakage process, which predicts a lognormal size distribution of the end products of a self-similar cascade process [35-38]. In ecology, the sequential breakage of ecological niche spaces has been proposed to explain patterns in the distributions of species abundance [39, 40]. To date, however, only indirect evidence has been consistent with this model [e.g., 40]. Many biological studies that have reported lognormal distributions [28, 31-34] have not shown that the processes underlying the distributions were characterized by self-similar geometries. Furthermore, there has been no evidence to support a linkage between lognormal distributions and self-similarity of the forms of individual organisms. Because the relationship between self-similarity and allometry has already been established by biological scaling theories [1, 3, 4, 9, 10, 14, 24], demonstration of a mechanism that connects self-similarity and lognormal distributions would lead to a unified understanding of self-similarity, allometry, and lognormal distributions in biology.

Plant vascular networks are a convenient model system for studying self-similarity of organismal forms [8, 10, 11, 13, 14, 24-26, 41, 42]. Here, we applied the

89 sequential breakage model of Kolmogorov [35] to self-similar plant forms and
90 hypothesized that the size distribution of the end products of a self-similar process (i.e.,
91 the lengths of the terminal twigs of a tree branch) would be approximated by a lognormal
92 distribution. The objective of the present study was to provide the first empirical evidence
93 that statistical self-similarity of the form of an individual organism generates a lognormal
94 distribution of the size of its terminal organs.
95

96 ## 2. The model

97 **(a) Multiplicative process**

98 The fact that a lognormal distribution can be generated by a stochastic, multiplicative
99 process was first formulized by Gibrat [43]. Let the size of a system (e.g., an organ,
100 organism, or population) at time t be $X(t)$. Each system is assumed to grow or shrink by a
101 randomly changing ratio $R(t)$ [29]:
102

103 $$X(t+1) = R(t)X(t) \quad (t = 0,1,...,n-1) \tag{2.1}$$
104

105 The log-transformed size of an object at final time n is then expressed as [29]:
106

107 $$\ln X(n) = \ln X(0) + \sum_{t=0}^{n-1} \ln R(t) \tag{2.2}$$
108

109 The term $\ln X(0)$, the logarithm of the initial size, is assumed to be a fixed value. The term
110 $\ln R(t)$ is then decomposed into two factors [44]:

$$\ln R(t) = M(t) + \varepsilon(t) \tag{2.3}$$

In equation (2.3), $M(t)$ is the mean of $\ln R(t)$ at time t, and $\varepsilon(t)$ is the deviation of $\ln R(t)$ from $M(t)$. The log-transformed final size is therefore [44]:

$$\ln X(n) = \ln X(0) + \sum_{t=0}^{n-1} M(t) + \sum_{t=0}^{n-1} \varepsilon(t) \tag{2.4}$$

The second term on the right-hand side of equation (2.4) has the same value for all the final objects and hence does not affect the shape of the final distribution. If values of $\varepsilon(t)$ are independent and come from the same distribution function, then the distribution of $\ln X(n)$ will asymptotically approach a normal distribution when n is large enough [44]. As discussed by Koch [29], the model described above is the mathematical equivalent of the sequential breakage process proposed by Kolmogorov [35] when $R(t)$ is the size ratio of an object after a single occurrence of breakage expressed as a fraction of the size before breakage.

(b) Application to plant form

We applied the sequential breakage process described above to the branching structure of Japanese elm trees (*Ulmus davidiana*), a temperate, deciduous tree species that grows new branches once a year. Following the plant model of Lindenmayer [45], we consider a tree branch to be the result of an iterative branching process. Let us consider a branch that

133 has many twigs. Let the age (denoted as T) of the oldest stem be n years ($T = n$). The stem
134 branches off several younger stems (child stems, age $T = n - 1$). Each of these child stems
135 further branches off younger stems ($T = n - 2$), and so on to the terminal 1-year-old twigs
136 at the branch periphery ($T = 1$).

137 The stem age described above is a centripetally ordered variable, which starts at
138 the terminal twigs ($T = 1$) and increases toward the oldest stem ($T = n$). To make our
139 model consistent with the terminology used in the sequential breakage model, we convert
140 T to centrifugal ordering (denoted as t), which increases toward the terminal twigs:

141

142 $$t = n - T \quad (t = 0,1,...,n-1) \tag{2.5}$$

143

144 The oldest stem is characterized by order $t = 0$ (the initial single stem segment), and 1-
145 year-old stems by order $t = n - 1$ (the terminal stem segments). The new ordering is
146 therefore consistent with the sequential breakage process (as is t in equations (2.1–2.4)),
147 in which one object progressively generates several objects (figure 1). In accordance with
148 the terminology used in river network analysis [46], we regard the order t as a scale
149 parameter that represents a sequence of scales within the system. Note that a single child
150 stem ($t = a + 1$) connected to a parent stem ($t = a$) differs in age and order from the parent
151 stem by 1, unlike the Horton–Strahler order [47], in which the two stems have the same
152 order.

153 As in the sequential breakage model, the length of a stem of order t is denoted by
154 $X(t)$, and the ratio of its length to the length of its parent is denoted by $R(t)$ (equation
155 (2.1)). Note that in the present model $R(t)$ could be greater than one when a child stem is

156 longer than its parent, unlike Kolmogorov's sequential breakage model, in which $R(t) < 1$.
157 Fractal-like objects in nature are characterized by statistical self-similarity, which
158 includes undescribed variations or errors at all scales [25, 41, 46]. We therefore allowed
159 $R(t)$ to vary among child stems of the same parent by decomposing $\ln R(t)$ into $M(t)$, the
160 mean of $\ln R(t)$ averaged within each order t, and $\varepsilon(t)$, the error term that allows variation
161 of lengths among the child stems within each order t (equation (2.3)). Statistical self-
162 similarity implies that probability distributions of a stochastic variable as measured over a
163 range of scales are similar to each other [46]. Our first hypothesis was that the branching
164 structure of elm trees is statistically self-similar. This hypothesis implies that the
165 distributions of the errors, $\varepsilon(t)$, should be similar at all values of t. If this condition is
166 satisfied, then equation (2.4) predicts that the distribution of the sum of $\varepsilon(t)$ will approach
167 a normal distribution when n is large enough. Our second hypothesis was therefore that
168 the distribution of the lengths of the terminal stems would approach a lognormal
169 distribution as n increases (figure 1).
170

171 ## 3. Materials and methods

172 **(a) Measurements**

173 The sampling site was a cool temperate natural riparian forest on the banks of the Urikari
174 River (42°52′N, 143°10′E; elevation: 75 m) in the city of Obihiro in northern Japan.
175 Three young Japanese elm trees (*Ulmus davidiana*) were selected on 9 July 2013. One
176 healthy branch with no significant damage was harvested from each tree (branches "1",
177 "2", and "3"); the ages of the branches were 7, 8, and 13 years, respectively. The
178 diameters at breast height of the trees from which the branches were harvested were 6.7,

179 2.4, and 2.1 cm for branches 1, 2, and 3, respectively. Their lengths (the maximum
180 distance between the branch base and the tip) were 150, 126, and 130 cm, respectively.
181 After harvesting, the branches were air-dried in a ventilated laboratory for three reasons:
182 (1) to prevent rotting and deterioration during storage; (2) to allow sufficient time for the
183 lengths of the samples to stabilize after harvesting; and (3) to be consistent with previous
184 analyses of the allometry of tree forms that have used dried materials [e.g., 48]. The
185 laboratory measurements were conducted from October 2013 to June 2014.

186 *U. davidiana* is a winter-deciduous species that elongates new shoots only once
187 per year. We determined the order (t) of each stem part by counting the number of
188 terminal bud scars from the tip to the base of each branch; a stereomicroscope (SZ61,
189 Olympus, Tokyo, Japan) was used to help discern the oldest, most basal bud scars. With
190 pruning shears or a saw, we decomposed each branch into “stem parts”, each of which
191 was of a different order (rectangles in figure 1), while simultaneously recording the
192 connection topology, i.e., all of the parent-child relationships among the stem parts
193 (figure 2). We defined terminal stem parts as new branches that had elongated and
194 matured in the preceding year. These terminal stem parts were 1-year-old shoots,
195 excluding the current-year shoots, which were still immature at the time of harvest in
196 early summer. We recognized a stem part as being alive when at least one green leaf was
197 attached to its descendant current-year shoots; only living stem parts were measured. We
198 did not measure small epicormic shoots, which can elongate to fill canopy gaps when
199 regular shoots die [49]. The healthy young branches that we sampled had no large
200 epicormic shoots.

We measured the lengths of long stem parts (> 10 cm) with a measuring tape and the lengths of short ones with a digital calliper (CD-15CPX, Mitutoyo, Kawasaki, Japan). We used length, rather than diameter, as an indicator of the size of a stem part for two reasons: (1) when the diameter was measured, the value depended on the small pressure of the calliper, especially for the small stem parts (< 1 mm diameter), and (2) the cross-section of the stem was neither an ideal circle nor an ellipse. Mainly for these two reasons, when we tried to measure the diameter of a same small stem repeatedly, the values we obtained were unstable. This instability would have caused considerable variability in the estimates of the sizes of small stem parts, especially if sized are recorded on a logarithmic scale. We therefore did not think that diameter was an appropriate metric of size in the present study, which focused on the variation of size on a logarithmic scale. In contrast, length was measured without contact between the calliper and a stem part when the calliper was set parallel to the main axis of a stem part. In addition, the length of a stem part was uniquely determined by the distance between the tip (i.e., the terminal bud scar) and the base of the stem part. We measured a total of 1968 stem parts (n = 813 from branch 1, n = 471 from branch 2, and n = 684 from branch 3), including 827 terminal stem parts (n = 422 from branch 1, n = 200 from branch 2, and n = 205 from branch 3; the electronic supplemental material, table S1, shows the number of data points at each order). Five small stem parts were lost before they could be measured, and their lengths were therefore not included in the analysis.

(b) Data analysis

223 We calculated the ratio of the length of each stem part to the length of its parent, $R(t)$
224 (equation (2.1)) and determined the value of $\varepsilon(t)$ (equation (2.3)) after calculating $M(t)$,
225 the mean of $\ln R(t)$ averaged over all order t stem parts on each branch. The distribution of
226 $\varepsilon(t)$ for each order of each branch was defined as the observed relative frequency
227 distribution of $\varepsilon(t)$ pooled over each order on each branch [46]. All statistical analyses
228 were performed with R ver. 3.3.1 [50].
229
230 **(c) Testing statistical self-similarity**
231 As shown in figure 1 (the model) and table S1 (the data structure), the total number of
232 stems at each order t increased exponentially toward the periphery on each branch. There
233 were hence only few stem parts on the proximal positions, whereas there were large
234 numbers of stem parts on the distal positions. According to the self-similar hypothesis,
235 the error distribution curve should converge to a common distribution as more data are
236 incorporated with increasing branching order. If the self-similar hypothesis is true, each
237 distribution would therefore be similar to the error distribution at the terminal (the most
238 distal) position. We used the bootstrap method proposed by Clauset et al. [51] to evaluate
239 the goodness-of-fit of the error distribution at each order ($\varepsilon(t)$) to the error distribution at
240 the terminal position. First, for each branch we compared the distribution of $\varepsilon(t)$ at each
241 order with the terminal error distribution by using the two-sample Kolmogorov–Smirnov
242 (K-S) test, and we then calculated the D statistic (hereafter called D_{obs}). The results
243 indicate that there was no significant difference between the $\varepsilon(t)$ at each order and the
244 terminal error distribution ($p > 0.25$ for all the branches). Next, random samples were
245 taken from the terminal error distribution to obtain the same sample size as the size of the

246 error distribution at each order by using the R function *sample* with replacement. For
247 each set of samples, a two-sample K-S test was performed to compare the sample
248 distribution with the terminal error distribution, and the resultant D statistic (hereafter
249 called D_{sim}) was calculated. This procedure was repeated 100,000 times, and the p-value
250 was defined as the fraction of D_{sim} values that were larger than D_{obs} [51]. We found two
251 pairs of data with tied ranks and tested whether the effect of these tied ranks significantly
252 affected the results. Because the true ratio of the lengths, which is a continuous variable,
253 should be different for each pair of stem parts, we added 10^{-12} to one value of $\varepsilon(t)$ from
254 each pair of $\varepsilon(t)$ values with tied ranks and repeated the above test: we obtained
255 essentially the same results, as shown in the Results section.
256
257 **(d) Testing lognormality**
258 The two-parameter lognormal distribution is defined by equation (3.1) [44]:
259
260 $$f(x) = \frac{N_{\mathrm{total}}}{x\sigma\sqrt{2\pi}} \exp\left(\frac{-\left(\ln x - m\right)^2}{2\sigma^2} \right) \tag{3.1}$$
261
262 In equation (3.1), x is the length of a terminal stem part (mm), $f(x)$ is the density of
263 terminal stem parts with length x, N_{total} is the total number of terminal stem parts on each
264 branch, and m (mean of ln x) and σ (standard deviation of ln x) are the curve-fitting
265 parameters. The parameters (m and σ) in equation (3.1) were estimated by maximum
266 likelihood estimation (MLE) by using the R package *fitdistrplus* [52]. The cumulative
267 distribution function (CDF) of the lognormal distribution is given by equation (3.2) [34]:

$$N(x) = \frac{N_{\text{total}}}{2}\left\{1 - \text{erf}\left[\frac{\ln x - m}{\sigma\sqrt{2}}\right]\right\} \quad (3.2)$$

In equation (3.2), $N(x)$ ($1 \leq N(x) \leq N_{\text{total}}$) is the cumulative number of all terminal stem parts as long as or longer than x. The function erf(z) is the Gauss error function and is defined by equation (3.3) [34]:

$$\text{erf}(z) = \frac{2}{\sqrt{\pi}}\int_0^z \exp(-y^2)dy \quad (3.3)$$

We then determined whether each one of the lognormal distribution function and normal distribution function was significantly better than the other in terms of goodness-of-fit to our dataset by using the Vuong likelihood ratio test [51, 53]. The CDF of the normal (Gaussian) distribution is given by equation (3.4):

$$N(x) = \frac{N_{\text{total}}}{2}\left\{1 - \text{erf}\left[\frac{x - m'}{\sigma'\sqrt{2}}\right]\right\} \quad (3.4)$$

The parameters of the normal distribution function (m' and σ') were also estimated by MLE. We then calculated the log likelihood ratio between the lognormal and normal distributions and tested whether the log of the ratio was significantly different from zero by using the equations described in Clauset et al. [51].

Next, after log-transformation of the data, several normality indices of the empirical distributions were compared with the theoretical normal distribution by using Monte Carlo methods. For each branch, the R function *rnorm* was used to generate normal random numbers with the same mean and variance as the empirical distribution and with the same sample size as the experimental data. The distributions of normality indices were then calculated (i.e., the 3^{rd}- and 4^{th}-order moments, skewness, kurtosis, and *D* statistic for the Lilliefors normality test [54], which in this case was equivalent to the good-ness-of fit test of Clauset et al. [51]. For each branch this simulation was repeated 100,000 times, and the distributions of these indices were calculated (hereafter called the simulated distributions of the indices). For each branch we tested whether each index of the empirical data was within the 95th percentile of the simulated distribution of the index. Several terminal stem parts on the same branch had exactly the same length (e.g., 2.23 mm) because of the limited resolution of the digital calliper (0.01 mm). We made the same adjustment as described above for these tied ranks, and we obtained essentially the same results as shown in the Results section.

4. Results

Our first hypothesis, that the branching structure of elm trees is statistically self-similar, was supported by the similarity of the observed empirical cumulative distributions of $\varepsilon(t)$ for different values of the scale parameter t (figure 3). The results of Clauset et al. [51]'s goodness-of-fit tests showed that there were no significant difference between the error distributions at each order and the terminal error distribution ($p > 0.17$ in all cases, see electronic supplemental material, table S2 for the p-value of each test). We tested whether

311 the distribution of the *p*-values that we obtained differed significantly from a uniform
312 distribution by using the two-sample K-S test and the R function *punif*. For this test, all
313 the *p*-values from the three branches were pooled ($N = 23$). The result was not significant
314 ($p = 0.41$), the indication being that the *p*-values were not significantly biased.

315 Our second hypothesis, that the distribution of the lengths of the terminal stems
316 would approach a lognormal distribution, was also supported by the good approximation
317 of the distributions of the lengths of terminal stem parts to a lognormal distribution
318 (figure 4). The Vuong likelihood ratio test showed that a lognormal distribution function
319 (the red curve in figure 4) was significantly preferred over a normal distribution function
320 (the blue curve in figure 4) ($p < 0.01$ for all the branches). However, after log-
321 transformation of the data, we found significant deviations from a theoretical normal
322 distribution on the basis of two statistical tests for branch-1 (table 1), which had the
323 lowest terminal branching order ($t = 6$) with the largest number of terminal stems ($N_{total} =$
324 422). For branch-2 ($t = 8$) and branch-3 ($t = 12$), which had larger terminal branching
325 orders, the distributions of the log-lengths were not significantly different from
326 theoretical normal distributions on the basis of any normality test. These results agree
327 with the model prediction that the distribution of the terminal twig lengths should
328 approach a lognormal distribution as the terminal branching order increases.
329

330 ## 5. Discussion

331 The results are consistent with the assertion that the within-scale error distribution is
332 often approximated by a lognormal rather than normal distribution in biological allometry
333 [30, 33]. However, a strictly lognormal distribution would be approached only if the

terminal branching order (t) approached infinity. In the case of such a distribution, the probability of observing some very small and some very large stems would increase as the sample size increases. Because this possibility is biologically unrealistic, there might be no strictly normal or lognormal distribution in real biological data if the sample size is sufficiently large and the order finite. In the present case, the terminal branching order of branch-1 (t = 6) may not have been large enough to satisfy the assumption of the model. Also, in the case of elm trees, our results seem to indicate that there was a lower limit to terminal stem size; the shortest terminal stem lengths on each branch were 1.30, 1.59, and 1.23 mm for branch-1, -2, and -3, respectively. That shorter stems were not found might reflect the fact that the smaller stems did not survive or that smaller buds became dormant. The observed deviation from a theoretical lognormal distribution in branch-1 may have been caused by these biological systematic deviations from strict lognormality.

Many empirical studies have demonstrated that variations in diverse biological phenomena are well approximated by lognormal distributions [28-34], but in those studies rigorous statistical tests were not performed. Those distributions may not have been theoretical lognormal distributions in the strict sense, even if the processes that underlay them were multiplicative. In this study, we proposed a lognormal distribution as a theoretically motivated simple model, because the underlying process was statistically self-similar and multiplicative. Including detailed biological factors, such as the limits of organ size, would further improve the predictive power of the model in future studies.

These results constitute an idealized approximation that we propose as a starting point. Plant form in nature is affected by wind, herbivory, and competition with neighbours [55, 56]. These factors can be expected to cause deviations from ideal self-

similarity and hence from lognormality. Further study is therefore needed to improve the analytical model before it can be applied in real-world situations.

Data Accessibility. All the raw data are available from the Dryad Digital Repository: doi:10.5061/dryad.776ht

Authors' Contributions. KK conceived of the study, designed the study, and collected the data. All authors analysed the data and were involved in writing the manuscript.

Competing interests. We have no competing interests.

Funding. This work was supported by Japan Society for the Promotion of Science Grant-in-Aid for Scientific Research number 25891001.

Acknowledgements. We thank the English Resource Center of the Obihiro University of Agriculture and Veterinary Medicine for help with proofreading this paper.

References

1. West, G.B., Brown, J.H. & Enquist, B.J. 1997 A general model for the origin of allometric scaling laws in biology. *Science* **276**, 122-126. (doi:10.1126/science.276.5309.122).
2. White, C.R. & Seymour, R.S. 2003 Mammalian basal metabolic rate is proportional to body mass(2/3). *Proc. Natl. Acad. Sci. USA* **100**, 4046-4049. (doi:10.1073/pnas.0436428100).
3. Savage, V.M., Deeds, E.J. & Fontana, W. 2008 Sizing up allometric scaling theory. *PLOS Comput. Biol.* **4**, e1000171. (doi:10.1371/journal.pcbi.1000171).
4. Okie, J.G. 2013 General models for the spectra of surface area scaling strategies of cells and organisms: fractality, geometric dissimilitude, and internalization. *Am. Nat.* **181**, 421-439. (doi:10.1086/669150).
5. Hirst, A.G., Glazier, D.S. & Atkinson, D. 2014 Body shape shifting during growth permits tests that distinguish between competing geometric theories of metabolic scaling. *Ecol. Lett.* **17**, 1274-1281. (doi:10.1111/ele.12334).

6 . White, C.R. & Kearney, M.R. 2014 Metabolic scaling in animals: methods, empirical results, and theoretical explanations. *Compr. Physiol.* **4**, 231-256. (doi:10.1002/cphy.c110049).

7 . Glazier, D.S., Hirst, A.G. & Atkinson, D. 2015 Shape shifting predicts ontogenetic changes in metabolic scaling in diverse aquatic invertebrates. *Proc. R. Soc. Lond. B* **282**, 20142302. (doi:10.1098/rspb.2014.2302).

8 . West, G.B., Brown, J.H. & Enquist, B.J. 1999 A general model for the structure and allometry of plant vascular systems. *Nature* **400**, 664-667. (doi:org/10.1038/23251).

9 . Enquist, B.J., Kerkhoff, A.J., Stark, S.C., Swenson, N.G., McCarthy, M.C. & Price, C.A. 2007 A general integrative model for scaling plant growth, carbon flux, and functional trait spectra. *Nature* **449**, 218-222. (doi:10.1038/nature06061).

10 . Enquist, B.J. & Bentley, L.P. 2012 Land plants: new theoretical directions and empirical prospects. In *Metabolic Ecology: A Scaling Approach.* (eds. R.M. Sibly, J.H. Brown & A. Kodric-Brown), pp. 164-187. Hoboken, USA, Wiley-Blackwell.

11 . Price, C.A., Weitz, J.S., Savage, V.M., Stegen, J., Clarke, A., Coomes, D.A., Dodds, P.S., Etienne, R.S., Kerkhoff, A.J., McCulloh, K., et al. 2012 Testing the metabolic theory of ecology. *Ecol. Lett.* **15**, 1465-1474. (doi:10.1111/j.1461-0248.2012.01860.x).

12 . Mori, S., Yamaji, K., Ishida, A., Prokushkin, S.G., Masyagina, O.V., Hagihara, A., Hoque, A., Suwa, R., Osawa, A., Nishizono, T., et al. 2010 Mixed-power scaling of whole-plant respiration from seedlings to giant trees. *Proc. Natl. Acad. Sci. USA* **107**, 1447-1451. (doi:10.1073/pnas.0902554107).

13 . Savage, V.M., Bentley, L.P., Enquist, B.J., Sperry, J.S., Smith, D.D., Reich, P.B. & von Allmen, E.I. 2010 Hydraulic trade-offs and space filling enable better predictions of vascular structure and function in plants. *Proc. Natl. Acad. Sci. USA* **107**, 22722-22727. (doi:10.1073/pnas.1012194108).

14 . Banavar, J.R., Cooke, T.J., Rinaldo, A. & Maritan, A. 2014 Form, function, and evolution of living organisms. *Proc. Natl. Acad. Sci. USA* **111**, 3332-3337. (doi:10.1073/pnas.1401336111).

15 . Ohtsuka, T., Saigusa, N., Iimura, Y., Muraoka, H. & Koizumi, H. 2016 Biometric-based estimations of net primary production (NPP) in forest ecosystems. In *Canopy Photosynthesis: From Basics to Applications* (eds. K. Hikosaka, Ü. Niinemets & N.P.R. Anten), pp. 333-351. Dordrecht, Springer Netherlands.

16 . Enquist, B.J., West, G.B. & Brown, J.H. 2009 Extensions and evaluations of a general quantitative theory of forest structure and dynamics. *Proc. Natl. Acad. Sci. USA* **106**, 7046-7051. (doi:DOI 10.1073/pnas.0812303106).

17 . West, G.B., Enquist, B.J. & Brown, J.H. 2009 A general quantitative theory of forest structure and dynamics. *Proc. Natl. Acad. Sci. USA* **106**, 7040-7045. (doi:DOI 10.1073/pnas.0812294106).

18 . Field, C. 1983 Allocating leaf nitrogen for the maximization of carbon gain - leaf age as a control on the allocation program. *Oecologia* **56**, 341-347. (doi:10.1007/bf00379710).

19 . Hikosaka, K., Kumagai, T.o. & Ito, A. 2016 Modeling canopy photosynthesis. In *Canopy Photosynthesis: From Basics to Applications* (eds. K. Hikosaka, Ü. Niinemets & N.P.R. Anten), pp. 239-268. Dordrecht, Springer Netherlands.

20 . Anten, N.P.R. 2016 Optimization and game theory in canopy models. In *Canopy Photosynthesis: From Basics to Applications* (eds. K. Hikosaka, Ü. Niinemets & N.P.R. Anten), pp. 355-377. Dordrecht, Springer Netherlands.

21 . Mooney, H.A. & Gulmon, S.L. 1979 Environmental and Evolutionary Constraints on the Photosynthetic Characteristics of Higher Plants. In *Topics in Plant Population Biology* (eds. O.T. Solbrig, S. Jain, G.B. Johnson & P.H. Raven), pp. 316-337. London, Macmillan Education UK.

22 . Mooney, H.A., Field, C., Gulmon, S.L. & Bazzaz, F.A. 1981 Photosynthetic capacity in relation to leaf position in desert versus old-field annuals. *Oecologia* **50**, 109-112. (doi:10.1007/Bf00378802).

23 . Niinemets, Ü. 2016 Within-canopy variations in functional leaf traits: structural, chemical and ecological controls and diversity of responses. In *Canopy Photosynthesis: From Basics to Applications* (eds. K. Hikosaka, Ü. Niinemets & N.P.R. Anten), pp. 101-141. Dordrecht, Springer Netherlands.

24 . Price, C.A., Enquist, B.J. & Savage, V.M. 2007 A general model for allometric covariation in botanical form and function. *Proc. Natl. Acad. Sci. USA* **104**, 13204-13209. (doi:10.1073/pnas.0702242104).

25 . Bentley, L.P., Stegen, J.C., Savage, V.M., Smith, D.D., von Allmen, E.I., Sperry, J.S., Reich, P.B. & Enquist, B.J. 2013 An empirical assessment of tree branching networks and implications for plant allometric scaling models. *Ecol. Lett.* **16**, 1069-1078. (doi:10.1111/ele.12127).

26 . Smith, D.D., Sperry, J.S., Enquist, B.J., Savage, V.M., McCulloh, K.A. & Bentley, L.P. 2014 Deviation from symmetrically self-similar branching in trees predicts altered hydraulics, mechanics, light interception and metabolic scaling. *New. Phytol.* **201**, 217-229. (doi:10.1111/nph.12487).

27 . Hunt, D. & Savage, V.M. 2016 Asymmetries arising from the space-filling nature of vascular networks. *Phys. Rev. E* **93**. (doi:10.1103/PhysRevE.93.062305).

28 . Preston, F.W. 1948 The commonness, and rarity, of species. *Ecology* **29**, 254-283.

29 . Koch, A.L. 1966 The logarithm in biology 1. Mechanisms generating the log-normal distribution exactly. *J. Theor. Biol.* **12**, 276-290. (doi:10.1016/0022-5193(66)90119-6).

30 . Kerkhoff, A.J. & Enquist, B.J. 2009 Multiplicative by nature: Why logarithmic transformation is necessary in allometry. *J. Theor. Biol.* **257**, 519-521. (doi:10.1016/j.jtbi.2008.12.026).

31 . Wakita, J.-i., Kuninaka, H., Matsuyama, T. & Matsushita, M. 2010 Size distribution of bacterial cells in homogeneously spreading disk-like colonies by *Bacillus subtilis*. *J. Phys. Soc. Jpn.* **79**, 094002. (doi:10.1143/jpsj.79.094002).

32 . Kattge, J. & Diaz, S. & Lavorel, S. & Prentice, C. & Leadley, P. & Bonisch, G. & Garnier, E. & Westoby, M. & Reich, P.B. & Wright, I.J., et al. 2011 TRY - a global database of plant traits. *Glob. Change Biol.* **17**, 2905-2935. (doi:10.1111/j.1365-2486.2011.02451.x).

33 . Xiao, X., White, E.P., Hooten, M.B. & Durham, S.L. 2011 On the use of log-transformation vs. nonlinear regression for analyzing biological power laws. *Ecology* **92**, 1887-1894. (doi:10.1890/11-0538.1).

34 . Kobayashi, N., Kuninaka, H., Wakita, J.-i. & Matsushita, M. 2011 Statistical features of complex systems -toward establishing sociological physics. *J. Phys. Soc. Jpn.* **80**, 072001. (doi:10.1143/jpsj.80.072001).

35 . Kolmogorov, A.N. 1941 Über das logarithmisch normale verteilungsgesetz der dimensionen der teilchen bei zerstückelung. *Dokl. Akad. Nauk SSSR* **31**, 99-101.

36 . de Wijs, H. 1951 Statistics of ore distribution. Part I: frequency distribution of assay values. *Geol. Mijnbouw* **13**, 365-375.

37 . Agterberg, F. 2007 New applications of the model of de Wijs in regional geochemistry. *Math. Geol.* **39**, 1-25. (doi:10.1007/s11004-006-9063-7).

38 . Yamamoto, K. & Wakita, J.-i. 2016 Analysis of a stochastic model for bacterial growth and the lognormality in the cell-size distribution. *J. Phys. Soc. Jpn.* **85**, 074004. (doi:10.7566/jpsj.85.074004).

39 . Sugihara, G. 1980 Minimal community structure - an explanation of species abundance patterns. *Am. Nat.* **116**, 770-787. (doi:10.1086/283669).

40 . Sugihara, G., Bersier, L.F., Southwood, T.R.E., Pimm, S.L. & May, R.M. 2003 Predicted correspondence between species abundances and dendrograms of niche similarities. *Proc. Natl. Acad. Sci. USA* **100**, 5246-5251. (doi:10.1073/pnas.0831096100).

41 . Mandelbrot, B.B. 1983 *The fractal geometry of nature*. San Francisco, USA, W. H. Freeman.

42 . Morse, D.R., Lawton, J.H., Dodson, M.M. & Williamson, M.H. 1985 Fractal dimension of vegetation and the distribution of arthropod body lengths. *Nature* **314**, 731-733. (doi:10.1038/314731a0).

43 . Gibrat, R. 1930 Une loi des réparations économiques: l'effet proportionnel. *Bulletin de la Statistique générale de la France* **19**, 469.

44 . Crow, E.L. & Shimizu, K. 1988 *Lognormal distributions: Theory and applications*. New York, USA, Marcel Dekker.

45 . Lindenmayer, A. 1968 Mathematical models for cellular interactions in development II. Simple and branching filaments with two-sided inputs. *J. Theor. Biol.* **18**, 300-315. (doi:10.1016/0022-5193(68)90080-5).

46 . Peckham, S.D. & Gupta, V.K. 1999 A reformulation of Horton's laws for large river networks in terms of statistical self-similarity. *Water. Resour. Res.* **35**, 2763-2777. (doi:10.1029/1999wr900154).

47 . Strahler, A.N. 1957 Quantitative analysis of watershed geomorphology. *EOS, Trans. Am. Geophys. Un.* **38**, 913-920. (doi:10.1029/TR038i006p00913).

48 . Shinozaki, K., Yoda, K., Hozumi, K. & Kira, T. 1964 A quantitative analysis of plant form-the pipe model theory: I. Basic analyses. *Jpn. J. Ecol.* **14**, 97-105.

49 . Ishii, H. & Ford, E.D. 2001 The role of epicormic shoot production in maintaining foliage in old *Pseudotsuga menziesii* (Douglas-fir) trees. *Can. J. Bot.* **79**, 251-264.

50 . R Core Team. 2016 *R: A language and environment for statistical computing. R Foundation for Statistical Computing, Vienna, Austria.*

51 . Clauset, A., Shalizi, C.R. & Newman, M.E.J. 2009 Power-law distributions in empirical data. *SIAM Rev.* **51**, 661-703. (doi:10.1137/070710111).

52 . Delignette-Muller, M.L. & Dutang, C. 2015 fitdistrplus: An R package for fitting distributions. *J. Stat. Softw.* **64**, 1-34.

53 . Vuong, Q.H. 1989 Likelihood ratio tests for model selection and non-nested hypotheses. *Econometrica* **57**, 307-333.

54 . Lilliefors, H.W. 1967 On the Kolmogorov-Smirnov test for normality with mean and variance unknown. *J. Am. Stat. Assoc.* **62**, 399-402. (doi:10.1080/01621459.1967.10482916).

55 . Muller-Landau, H.C., Condit, R.S., Chave, J., Thomas, S.C., Bohlman, S.A., Bunyavejchewin, S., Davies, S., Foster, R., Gunatilleke, S., Gunatilleke, N., et al. 2006 Testing metabolic ecology theory for allometric scaling of tree size, growth and mortality in tropical forests. *Ecol. Lett.* **9**, 575-588. (doi:10.1111/j.1461-0248.2006.00904.x).

56 . Duursma, R.A., Makela, A., Reid, D.E.B., Jokela, E.J., Porte, A.J. & Roberts, S.D. 2010 Self-shading affects allometric scaling in trees. *Funct. Ecol.* **24**, 723-730. (doi:10.1111/j.1365-2435.2010.01690.x).

Table and figure legends (one table and four figures)

Table 1					
			The percentile of the indices and *D* statistic simulated from the theoretical normal distribution		
Indices	Log-transformed our dataset	Significance	Lower limit of 95% precentile	Median value	Upper limit of 95% percentile
Branch -1					
3rd-order moment	15.23	N.S.[a]	13.56	14.94	16.39
4th-order moment	46.32	N.S.	38.33	43.67	49.55
Skewness	0.54	$P < 0.05$	-0.23	0.00	0.23
Kurtosis	3.10	N.S.	2.59	2.96	3.51
D statistic (K-S test)	0.061	$P < 0.05$	---[b]	0.030	0.044
Branch -2					
3rd-order moment	30.29	N.S.	26.47	30.31	34.52
4th-order moment	110.58	N.S.	92.60	111.12	132.72
Skewness	-0.02	N.S.	-0.34	0.00	0.34
Kurtosis	2.59	N.S.	2.44	2.93	3.75
D statistic (K-S test)	0.042	N.S.	---	0.043	0.063
Branch- 3					
3rd-order moment	17.09	N.S.	14.74	17.03	19.57
4th-order moment	52.84	N.S.	43.30	52.61	63.63
Skewness	0.07	N.S.	-0.33	0.00	0.33
Kurtosis	2.49	N.S.	2.45	2.93	3.74
D statistic (K-S test)	0.054	N.S.	---	0.042	0.063

[a]Not significant ($p > 0.05$). [b]One-sided tests (*D* statistics).

Table 1. The percentile of the indices and *D* statistic simulated from the theoretical normal distribution function and those of our log-transformed datasets.

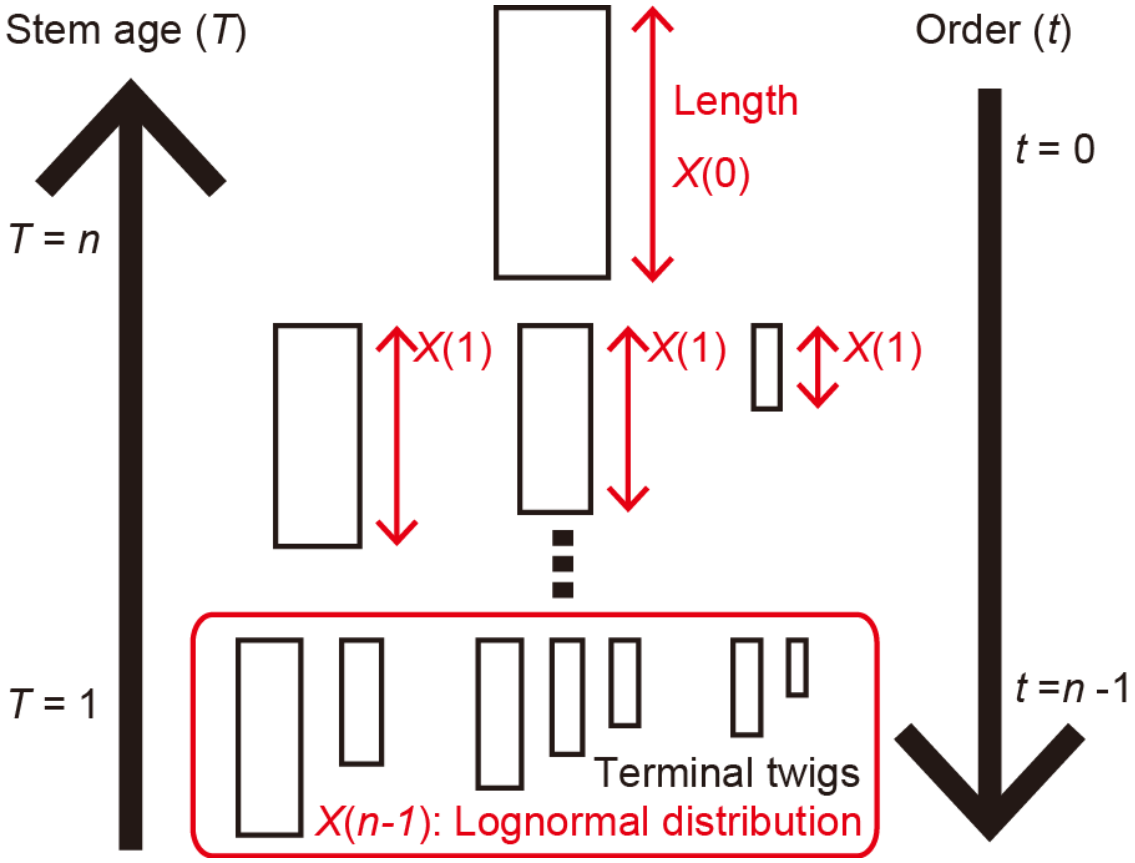

Figure 1. Model of the tree branching structure. The centrifugal order (t) in the sequential breakage model increases with decreasing age of the stem parts (T).

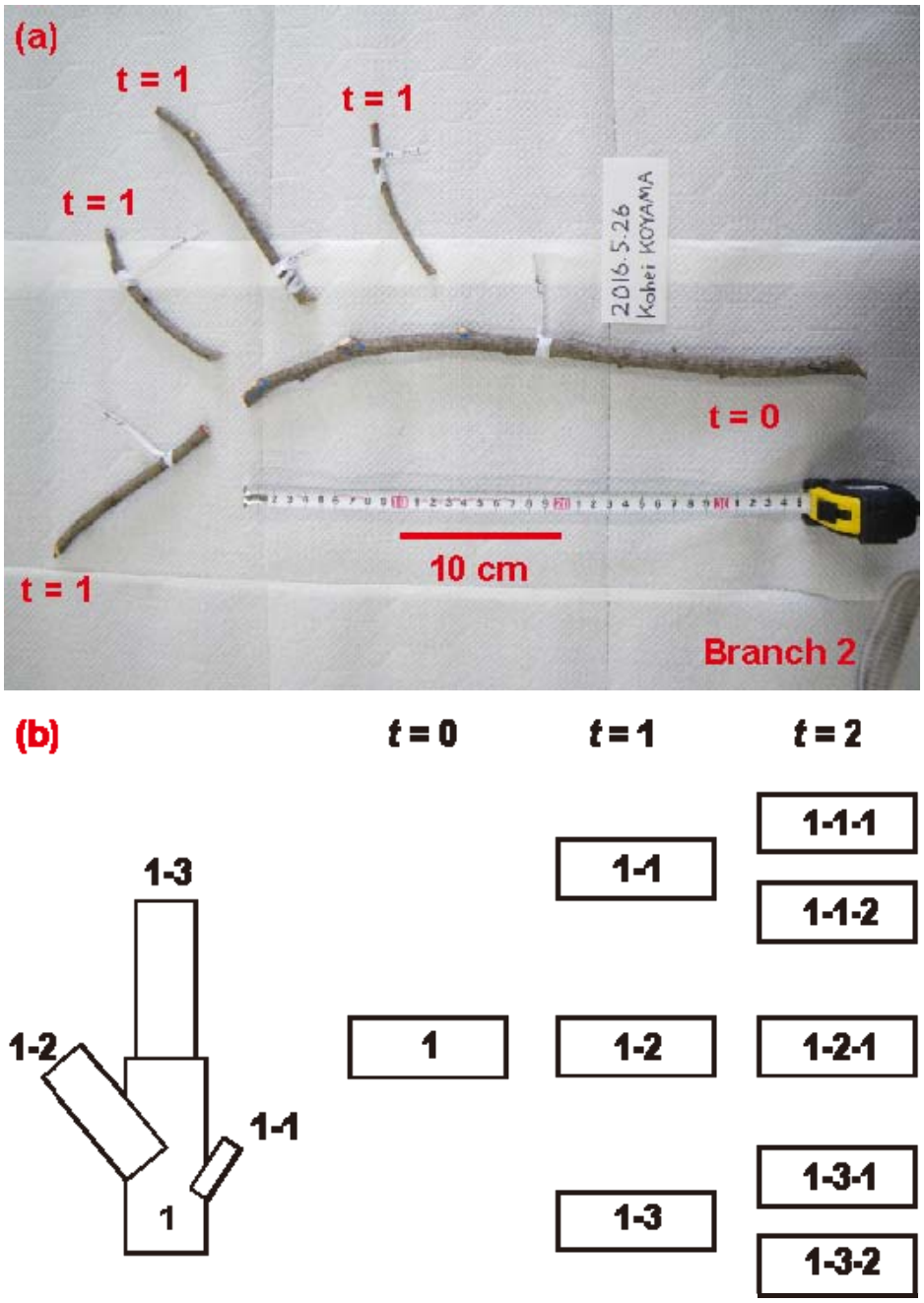

505

506 **Figure 2.** Decomposition of stem parts. **(a)** A photograph of stored samples taken on 26

507 May 2016 during preparation of the manuscript. **(b)** Labelling procedure; numbers within

508 each generation are ordered from the proximal to the distal position of each parent stem

509 part. Immediately after decomposition, each stem part was stored in a labelled envelope.

510

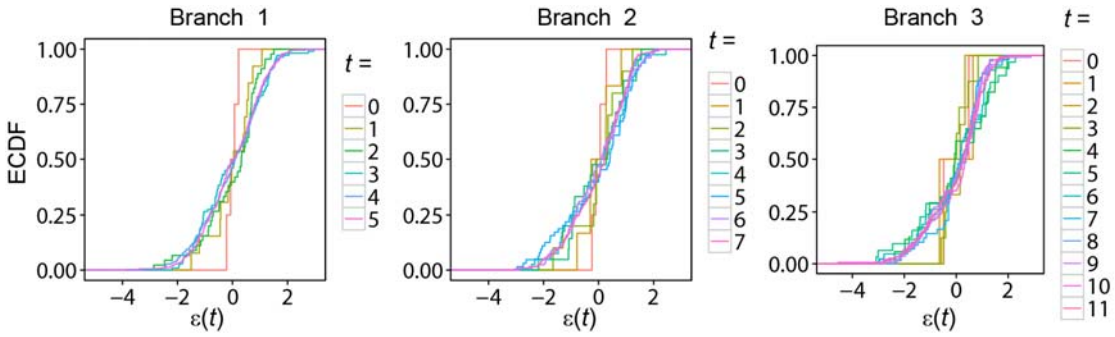

Figure 3. Empirical cumulative distribution functions (ECDFs) of $\varepsilon(t)$. Different colour lines indicate different orders (t) on each branch. Statistical self-similarity is evidenced by the fact that the distributions of different orders collapsed into approximately a single curve. The deviations of the initial orders were a consequence of the fact that there were few child stem parts.

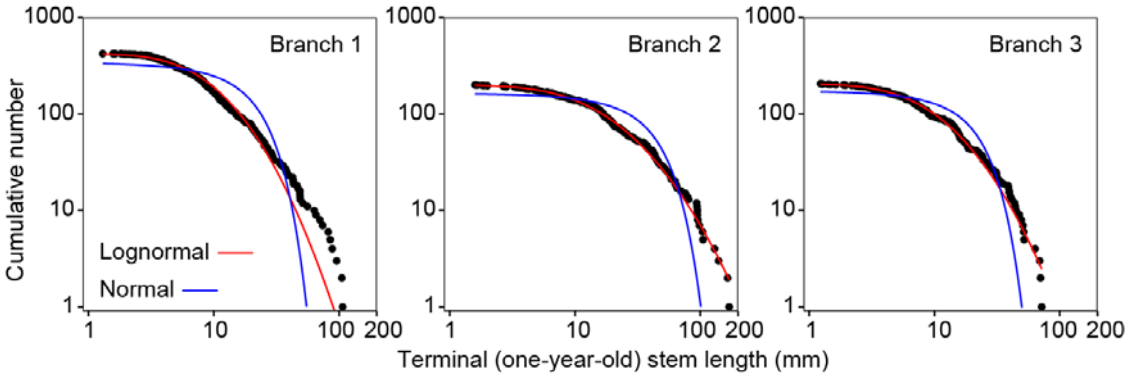

Figure 4. Distributions of the lengths of terminal twigs (i.e., 1-year-old stem parts). Red curves show the cumulative distribution functions (CDFs) of lognormal distributions (equation (3.2); branch 1: $N_{\text{total}} = 422$, $m = 2.19$, $\sigma = 0.815$; branch 2: $N_{\text{total}} = 200$, $m = 2.80$, $\sigma = 0.997$; branch 3: $N_{\text{total}} = 205$, $m = 2.27$, $\sigma = 0.889$) and the blue curves show the CDFs of the normal distributions (equation (3.4); branch 1: $m = 13.1$, $\sigma = 14.8$; branch 2: $m = 26.5$, $\sigma = 28.9$; branch 3: $m = 14.3$, $\sigma = 13.7$). The parameters of both the lognormal and normal CDFs were determined by using the maximum likelihood estimation.